

Visualization of Strain-Induced Landau Levels in a Graphene - Black Phosphorus Heterostructure

*Thi-Hai-Yen Vu, Pin Lyu, Na Hyun Jo, Chi Xuan Trang, Qile Li, Aaron Bostwick, Chris Jozwiak, Eli Rotenberg, Jiong Lu, Michael S. Fuhrer, Mark T. Edmonds**

T. H. Y. Vu, C. X. Trang, Q. Li, M. S. Fuhrer, M. T. Edmonds

School of Physics and Astronomy

Monash University

Clayton. VIC 3800, Australia

E-mail: Mark.Edmonds@monash.edu

T. H. Y. Vu, C. X. Trang, Q. Li, M. S. Fuhrer, M. T. Edmonds

ARC Centre for Future Low Energy Electronics Technologies

Monash University

Clayton, VIC 3800, Australia

M. T. Edmonds

ANFF-VIC Technology Fellow

Melbourne Centre for Nanofabrication

Victorian Node of the Australian National Fabrication Facility

Clayton, VIC 3168, Australia

N. H. Jo, A. Bostwick, C. Jozwiak, E. Rotenberg

Advanced Light Source

Lawrence Berkeley National Laboratory

Berkeley, CA 94720, USA

P. Lyu, J. Lu

Department of Chemistry

National University of Singapore

Singapore, 117543 Singapore

P. Lyu, J. Lu

Centre for Advanced 2D Materials and Graphene Research Centre

National University of Singapore

Singapore, 117546 Singapore

Keywords: graphene, nano-angle resolved photoemission spectroscopy, landau levels, pseudo-magnetic field.

Abstract – Strain-induced pseudo magnetic fields offer the possibility of realizing zero magnetic field Quantum Hall effect in graphene, possibly up to room temperature, representing a promising avenue for lossless charge transport applications. Strain engineering on graphene has been achieved *via* random nanobubbles or artificial nanostructures on the substrate, but the highly localized and non-uniform pseudomagnetic fields can make spectroscopic probes of electronic structure difficult. Heterostructure engineering offers an alternative approach: By stacking graphene on top of another van der Waals material with large lattice mismatch at a desired twist angle, it is possible to generate large strain-induced pseudo magnetic fields uniformly over the entire heterostructure. Here, we report using nano-angle resolved photoemission spectroscopy (nano-ARPES) to probe the electronic bandstructure of a graphene/black phosphorus heterostructure (G/BP). By directly measuring the iso-energy contours of graphene and black phosphorus we determine a twist angle of 20-degrees in our heterostructure. High-resolution nano-ARPES of the graphene bands near the Fermi level reveals the emergence of flat bands located within the Dirac cone. The spacing of the flat bands is consistent with Landau level formation in graphene, and corresponds to a pseudo-field of 11.36 T. Our work provides a new way to study quantum Hall phases induced by strain in 2D materials and heterostructures.

1. Introduction

Graphene is a promising platform to study novel electronic phases due to its linear band structure and massless Dirac-like fermions^[1-5], which allow the quantum Hall effect (QHE) to be measured even at room temperature under a strong magnetic field^[6]. In the QHE, electrons moving in a uniform magnetic field will travel in quantized cyclotron orbits with discrete energy levels called Landau levels (LLs). In order to observe LLs, the energy gaps between LLs must be larger than the thermal energy and the phenomenological scattering time must be longer than the period of the cyclotron orbits. Therefore, strong magnetic fields are typically required to satisfy these conditions. Yet, the massless Dirac-like behaviour of graphene provides a potential avenue to realise LLs without the need for strong magnetic fields as the unique Dirac Hamiltonian allows for not only scalar potentials but also vector potentials which can be generated by e.g. lattice deformations. If a non-uniform distortion is applied to the graphene lattice it shifts the graphene Dirac cones at K and K' in two opposite directions and thus generates a pseudo magnetic field (PMF)^[7]. Similar to the case of a real magnetic field, the LLs are isospin (K and K' valley) degenerate, however the PMF direction is opposite for the two isospins (valleys). The ability to tailor the strain-induced PMF in graphene has received intense interest because it generates an energy gap with the potential of realising a zero magnetic field of the QHE with applications in lossless charge transport. Unlike the regular

QHE where time reversal symmetry is broken, zero magnetic field QHE is able to generate two counter-circulating topological edge states without broken time reversal symmetry^[8].

So far, evidence of LLs generated by PMF in strained graphene has mainly been observed in highly localized regions such as random nano-bubbles or artificial nanostructures using scanning tunnelling microscopy/spectroscopy (STM/STS)^[9,10]. Yet, as a van der Waals 2D material, graphene can be utilised in heterostructure engineering by stacking one monolayer on top of another van der Waals material to form a heterostructure, thus providing a new approach to strain engineering and the tailoring of the sample wide PMF ^[11–16]. In 2018, Liu et al. reported that when graphene is stacked on black phosphorus (BP), the large lattice mismatch between them creates a shear strained superlattice which gives rise to a periodic PMF across the entire heterostructure^[17]. More interestingly, the intensity and spatial distribution of PMF can be tuned as a function of the twist angle between the graphene and black phosphorus. Using scanning tunnelling spectroscopy (STS), they observed strong peaks in the dI/dV spectra and determined they were strain-induced LLs. Yet, as a local probe STS measures local density of states and is not able to measure band dispersion in momentum space. Furthermore, dI/dV measures states from both graphene and black phosphorus and it is often difficult to disentangle them. To further elucidate the strain-induced PMF in a graphene/black phosphorous (G/BP) heterostructure requires direct measurement of the band dispersion of LLs in momentum space.

ARPES is a momentum and energy resolved technique that has proven to be a powerful tool in directly studying the electronic band structure of a variety of materials, including graphene^[18–20], 3D topological insulators^[21–23], 2D quantum spin Hall insulators^[24–26] and magnetic topological insulators^[27] and can also be used to probe thickness, temperature and electric-field induced phase transitions^[28,29]. However, only limited studies of quantum Hall states have been performed, since ARPES is strictly incompatible with external magnetic fields, as the magnetic field would perturb essential crystal momentum information carried by the emitted photoelectrons. Yet, because the pseudo-magnetic fields are intrinsic to the heterostructure and interact with the Dirac electrons inside the material, ARPES can be used to measure systems with pseudo-magnetic fields^[30]. In addition, ARPES gives direct access to the valley (isospin) degree of freedom of the pseudo-LLs by probing K and K' points of graphene. Previously, ARPES measurement on strained triangular nanoprisms of graphene on SiC reported evidence of LL formation, but was performed by spatially averaging over both unstrained and strained regions of graphene due to the large beam size of 1 mm^[30]. Hence, it is of fundamental importance to measure LLs in graphene that occur uniformly across the whole sample. In this report, we investigated the electronic bandstructure of a G/BP heterostructure with a twist angle of 20 degrees using nano-ARPES. The energy dispersion of LLs in momentum space was visualised and the influence of strain to the original band structure of graphene and black phosphorus are also discussed.

2. Results and discussion

Figure 1a and **b** show a schematic and an optical image of our G/BP heterostructure. Due to the poor air-stability of black phosphorus, we transferred chemical vapour deposition (CVD) grown graphene on top of the exfoliated black phosphorus in a Ar-filled glovebox to completely encapsulate it in order to prevent oxidation of the black phosphorus^[31,32]. The encapsulation allows the sample to be annealed at 200°C in ultra-high vacuum, to remove surface contamination without degrading the BP. To prevent charging during photoemission measurements the graphene was grounded near the edges of the Si wafer with conductive epoxy. To locate the black phosphorus flake in the ARPES chamber, we used scanning

photoemission microscopy (SPEM) to map the real space distribution of generated photoelectrons from the valence band of graphene and black phosphorus, and also the black phosphorus P 2*p* core level. This was measured at photon energy $h\nu = 200$ eV using a beam spot with the size of approximately 1 μm . Figure 1c and d show the SPEM maps of the valence band and P 2*p* core level respectively, exhibiting uniform signal across the whole flake. Importantly, the P 2*p* spectrum (Figure 1e) shows only a single doublet reflecting the P 2*p*_{3/2} and P 2*p*_{1/2} spin-split components with peak positions of 129.90 eV and 130.80 eV respectively, in good agreement with literature values of pristine black phosphorus^[31]. The absence of additional components at higher binding energy, which would represent oxide components^[31] indicates the black phosphorus is pristine. Before performing ARPES measurements we also measured the C 1*s* core level at $h\nu = 350$ eV to confirm the graphene is free of contamination, as shown in Figure 1f. We fit the C1*s* core level of graphene using the Doniach Sunjic function to reflect the characteristic asymmetric line shape of sp² bonded carbon with binding energy of 284.6 eV. There is a small shoulder at 285.3 eV, possibly due to some remnant polymer residue from the transfer process. However, the peak is small and is almost negligible compared to reported results.^[33–36]

Since we have confirmed that the G/BP heterostructure is pristine, we turn to angle-resolved photoemission measurements to measure the electronic bandstructure of the heterostructure utilising nano-ARPES with a beam size of ~ 1 μm . The small beam size allows measurements of the band structure on a single graphene domain, and it also minimises the effects of wrinkles formed during the transfer process of CVD graphene onto black phosphorus^[17].

To determine the twist angle in our G/BP heterostructure, we measured iso-energy maps at $h\nu = 150$ eV at selected binding energies in order to observe how the graphene and black phosphorus Brillouin zones align with respect to each other. In real space, the twist angle, θ , of the heterostructure is defined as the angle between the zigzag direction of graphene and the zigzag direction of BP. Converting to momentum space, the twist angle is determined by the angle between K- Γ -K' direction of graphene and the Γ -Y direction of black phosphorus. A schematic of the G/BP heterostructure in real space and their corresponding first Brillouin zone in k space are presented in **Figure 2a** and b. Figure 2c-e are the iso-energy cuts taken at Fermi level, BE = 0.5 eV and BE = 1 eV below Fermi level, respectively. In the iso-energy map taken at the Fermi energy (Figure 2c), the only spectral weight occurs at discrete points in momentum space that correspond to the K and K' points of the hexagonal Brillouin zone of the graphene (we overlay the hexagonal graphene Brillouin zone in orange for clarity). As shown in Figure 2f, the band dispersion in k space exhibits two characteristic Dirac cones of graphene, confirming the high symmetry K- Γ -K' direction. Along this direction, we only observe half of the Dirac cone instead of the full Dirac cone due to the dark corridor effect^[37].

Due to the semiconducting nature of black phosphorus, we need to probe deeper in binding energy below the Fermi level to detect the black phosphorus bands near Γ , as shown in Figure 2d and e. Here, the features originating from the black phosphorus valence band appear stronger. From the energy dispersion curves, the valence band maximum lies around BE = 0.15 eV below the Fermi level at the Γ point. Along the high symmetry direction shown in Figure 2g, the second Γ is observed at 1.8 \AA^{-1} from the first Γ , suggesting the Γ -Y direction of black phosphorus. We have added a blue rectangle to aid visualization of the black phosphorus 2D surface Brillouin zone. Along the other high symmetry direction shown in Figure 2h, there are four satellite bands appearing at ~ 0.9 eV below Fermi, indicating the Γ -X direction of black phosphorus^[38]. The K- Γ -K' direction of graphene and the Γ -Y direction of black phosphorus are also marked in red lines in Figure 2e. Now we can determine the twist angle by comparing

the misalignment between the Brillouin zones of the graphene and black phosphorus, which yields a twist angle of 20 ± 0.5 degrees. This twist angle and large lattice mismatch between graphene and black phosphorus leads to a Moiré superlattice whose wavelengths are related to both lattice mismatch (δ_i) and twist angle (θ) as follows:

$$\lambda_1 = \frac{b_2}{\sqrt{\delta_2^2 + 2(1 + \delta_2)(1 - \cos\theta)}} \quad (1)$$

$$\lambda_2 = \frac{b_1}{\sqrt{\delta_1^2 + 2(1 + \delta_1)(1 - \cos\theta)}} \quad (2)$$

where the lattice constants of BP are $b_1 = 0.331$ nm, $b_2 = 0.438$ nm and the lattice constant of graphene $a = 0.246$ nm. Hence, the Moiré wavelength of the superlattice formed in 20-degree twisted G/BP heterostructure are calculated to be $\lambda_1 = 1.24$ nm and $\lambda_2 = 0.62$ nm. Note, that the strain distributions in the graphene lattice are mostly affected by the longer Moiré wavelength λ_1 . Even though the shape of the graphene band dispersion along the K- Γ -K' direction retains the same characteristic linear band dispersion and Dirac cone feature, the distance from Γ to K and K' is modified due to the Moiré superlattice from the standard value of 1.703 \AA^{-1} to 1.72 and 1.65 \AA^{-1} (Figure 2c), respectively. These differences in lattice constant are larger than the experimental momentum resolution of 0.01 \AA^{-1} . These values correspond to lattice constants of 0.243 nm and 0.253 nm in real space, and strain value of 1% and 3% respectively in reasonable agreement with previous STM study^[17]. Meanwhile, the black phosphorus bands remain mostly unchanged. The black phosphorus bands show rectangular symmetry with $d_{\Gamma-X} = 0.69 \text{ \AA}^{-1}$ and $d_{\Gamma-Y} = 0.91 \text{ \AA}^{-1}$. From the dispersion of the valence band at Γ we can determine the hole effective masses in the Γ -X direction (m_{x^*}/m_0) to be 0.17 and the Γ -Y direction (m_{y^*}/m_0) to be 0.71 which are consistent with values in bulk crystals^[39].

To confirm whether the pseudo-magnetic field induced by the twisted G/BP heterostructure gives rise to flat-dispersionless LLs near the Fermi energy, we perform high resolution ARPES measurements at $h\nu = 60$ eV in **Figure 3**. In Figure 3a, the ARPES data show the expected linear Dirac cone of graphene, with the Dirac point located above the Fermi level. Linear fitting of the Dirac band dispersion yields a Fermi velocity, $v_F = 1.06 \pm 0.2 \times 10^6 \text{ ms}^{-1}$. Linear extrapolation of the Dirac band, using $E = \hbar v_F k_F$ and the Fermi velocity of $1.06 \pm 0.2 \times 10^6 \text{ m s}^{-1}$ yields a Dirac point 42 ± 15 meV above the Fermi level, indicating the graphene is slightly *p*-doped. Within the Dirac cone new flat bands emerge at discrete energies near the Fermi level (Figure 3b), the first flat band is observed at 81 meV below the Fermi level. The LLs are confined to the Dirac cone as the harmonic oscillator parts of the eigenfunction in a magnetic field localise the momentum relative to the K and K' points but the K, K' momentum remains^[40].

To determine the binding energy of these bands more clearly, we extracted the energy distribution curve (EDC) at the K point as shown in Figure 3c, after being divided by the Fermi function and subtracting the background. The positions of the flat bands are extracted by fitting the peaks in the EDC with a series of Gaussian peaks, with the peak maxima marked by arrows in Figure 3c and labelled from LL1 to LL6. Whilst, LL1, LL4-6 show only a single peak, some additional splitting of the flat bands is observed at the LL2 and LL3 peaks, and may arise as a result of the non-uniform PMF generated in this heterostructure. By plotting the position of these flat bands with respect to the integer Landau Level index, we observe a \sqrt{n} spacing as shown in Figure 3d, which is expected for LLs due to the massless Dirac fermions^[2].

In graphene the energies of these pseudo- LLs are expressed by the following equation:

$$E_N - E_D = \text{sgn}(N)\sqrt{2e\hbar v_F^2 B_S} \times \sqrt{|N|} \quad (3)$$

where $E_N - E_D$ is the energy of N^{th} Landau level and Dirac point with respect to the Fermi level, \hbar is the Planck constant, $v_F = 1.06 \times 10^6 \text{ ms}^{-1}$ is the graphene Fermi velocity measured for this heterostructure and B_S is PMF.

In Figure 3d the energy levels are plotted as a function of LLs index (red points) with the Dirac point indicated with a black circle and show a linear dependence. We then fit the data to Equation (3), shown as a solid line, and from that we can extract the pseudo-magnetic field, which yields $B_S = 11.36 \pm 0.3 \text{ T}$. From the calculated pseudo-magnetic field, we can also predict the magnetic length of the LLs which should be the width of the Gaussian in real space and given by:

$$l_B = \sqrt{\frac{\hbar}{eB_S}} \quad (4)$$

This gives a magnetic length of 76 \AA , which converting to momentum space ($k_B = 1/2l_B$) gives $k_B = 0.007 \text{ \AA}^{-1}$. Experimentally, we observe LLs that are significantly broader in momentum than the predicted values, due to momentum resolution limits and possibly disorder in our sample.

3. Conclusion

In conclusion, we have investigated the energy dispersion in momentum space of a twisted G/BP heterostructure using nano-ARPES. We use the misalignment of the graphene and black phosphorus iso-energy contours to directly determine the twist angle of the heterostructure. We demonstrate that the strain showed no influence on the black phosphorus band structure but it changed the graphene band structure significantly. The formation of a discrete set of LLs was observed inside the graphene Dirac cone, with the spacing corresponding to a strain-induced pseudo-field of 11.36 T . The spacing of the 1^{st} Landau level relative to the 0^{th} Landau level is 123 meV , which is significantly larger than room temperature $kT = 25 \text{ meV}$. These results demonstrate that nano-ARPES is an excellent tool for studying strain-induced quantum Hall phases in other 2D Dirac materials and heterostructures. The direct access of ARPES to the valley (isospin) degree of freedom of the pseudo-LLs will be useful in future studies searching for isospin symmetry breaking due to interactions in strong PMF. Whilst, application of a real magnetic field in ARPES remains challenging, the recent emergence of a variety of van der Waals 2D ferromagnets^[41] opens the possibility of directly imaging spin- and isospin-resolved LLs using nano-ARPES to probe the interplay of spin and orbital degrees of freedom with PMF and exchange interactions.

4. Methods

Sample fabrication

Black phosphorus flakes were mechanically exfoliated onto a silicon dioxide wafer from bulk crystal (HQ Graphene) using blue tape, then suitable flakes are selected using optical microscopy. Next, the high-quality CVD-grown monolayer graphene is transferred on top of the black phosphorus and covers the whole SiO_2 wafer using semi-dry transfer method. The

whole process is performed in an Ar-filled glovebox to prevent degradation of the black phosphorus.

Nano ARPES measurement

The samples were transported to the Microscopic and Electronic Structure Observatory (MAESTRO) beamline at the Advanced Light Source in a sealed Ar-filled container. They were mounted onto a sample holder using conducting epoxy inside a glovebox connected to the load lock, before being introduced into ultra-high vacuum. The samples were annealed at 200 °C for 6 hours in the preparation chamber ($<1 \times 10^{-10}$ torr) prior to the measurement to remove residual absorbents. The beam spot size is 1 μm , approximately. The ARPES measurements were performed with capillary focusing using several photon energies between 60 to 200 eV. The P 2p and C 1s core levels were measured photon energies of 200 eV and 350 eV, respectively. The data were collected using a hemispherical Scienta R4000 electron analyser. All measurements were performed at 20K. For the high-resolution energy scan of the graphene bands the energy and momentum resolution were 15 meV and $\approx 0.01 \text{ \AA}^{-1}$ respectively.

Acknowledgements

T. H. Y. V, M. S. F, and M. T. E acknowledge funding support from DP200101345. M. T. E., C. X. Trang and Q. Li acknowledge travel funding provided by the International Synchrotron Access Program (ISAP) managed by the Australian Synchrotron, part of ANSTO, and funded by the Australian Government. M. T. E. acknowledges funding support from the ANFF-VIC Technology Fellow program. Q. Li acknowledges funding support from the AINSE postgraduate award. This research used resources of the Advanced Light Source, which is a DOE Office and Science User Facility under contract no. DE-AC02-05CH11231. This work was performed in part at the Melbourne Centre for Nanofabrication (MCN), the Victorian Node of the Australian National Fabrication Facility (ANFF). J. L. acknowledges the support from MOE Tier 2 grants (MOE2019-T2-2-044 and MOE-T2EP10221-0005). E. R. and N. H. Jo were supported by the U.S. Department of Energy, Office of Science, National Quantum Information Science Research Centers, Quantum Systems Accelerator.

References

- [1] K. S. Novoselov, D. Jiang, F. Schedin, T. J. Booth, V. V. Khotkevich, S. V. Morozov, A. K. Geim, *Proc. Natl. Acad. Sci. U. S. A.* **2005**, *102*, 10451.
- [2] A. K. Geim, K. S. Novoselov, *Nat. Mater.* **2007**, *6*, 183.
- [3] A. H. C. Neto, *Rev. Mod. Phys.* **2009**, *81*, 109.
- [4] K. S. Novoselov, A. K. Geim, S. V. Morozov, D. Jiang, M. I. Katsnelson, I. V. Grigorieva, S. V. Dubonos, A. A. Firsov, *Nature* **2005**, *438*, 197.
- [5] Y. Lei, T. Zhang, Y. Lin, T. Granzier-nakajima, G. Bepete, D. A. Kowalczyk, Z. Lin, D. Zhou, T. F. Schranhamer, A. Dodda, A. Sebastian, Y. Chen, Y. Liu, G. Pourtois, T. J. Kempa, B. Schuler, M. T. Edmonds, S. Y. Quek, U. Wurstbauer, S. M. Wu, N. R. Glavin, S. Das, S. P. Dash, J. M. Redwing, J. A. Robinson, M. Terrones, *ACS Nanosci. Au* **2022**, *0*, pp.
- [6] K. S. Novoselov, Z. Jiang, Y. Zhang, S. V. Morozov, H. L. Stormer, U. Zeitler, J. C. Maan, G. S. Boebinger, P. Kim, A. K. Geim, *Science (80-.)* **2007**, *315*, 1379.
- [7] T. Low, F. Guinea, *Nano Lett.* **2010**, *10*, 3551.
- [8] M. I. Katsnelson, A. K. Geim, *Nat. Phys.* **2010**, *6*, 1.

- [9] N. a Gershenfeld, I. L. Chuang, W. S. Warren, G. D. Fuchs, V. V Dobrovitski, D. M. Toyli, F. J. Heremans, D. D. Awschalom, F. Jelezko, T. Gaebel, I. Popa, A. Gruber, J. Wrachtrup, V. B. Braginsky, F. Y. Khalili, N. Imoto, H. a Haus, Y. Yamamoto, K. S. Thorne, R. W. P. Drever, M. Zimmermann, S. D. Bartlett, G. J. Pryde, H. M. Wiseman, P. Neumann, J. Beck, I. H. Deutsch, *Science* (80-.). **2010**, 544.
- [10] Y. Jiang, J. Mao, J. Duan, X. Lai, K. Watanabe, T. Taniguchi, E. Y. Andrei, *Nano Lett.* **2017**, 17, 2839.
- [11] N. P. Kazmierczak, M. Van Winkle, C. Ophus, K. C. Bustillo, S. Carr, H. G. Brown, J. Ciston, T. Taniguchi, K. Watanabe, D. K. Bediako, *Nat. Mater.* **2021**, 20, 956.
- [12] G. H. Ahn, M. Amani, H. Rasool, D. H. Lien, J. P. Mastandrea, J. W. Ager, M. Dubey, D. C. Chrzan, A. M. Minor, A. Javey, *Nat. Commun.* **2017**, 8, 1.
- [13] Y. Han, K. Nguyen, M. Cao, P. Cueva, S. Xie, M. W. Tate, P. Purohit, S. M. Gruner, J. Park, D. A. Muller, *Nano Lett.* **2018**, 18, 3746.
- [14] S. Dai, Y. Xiang, D. J. Srolovitz, *Nano Lett.* **2016**, 16, 5923.
- [15] J. S. Alden, A. W. Tsen, P. Y. Huang, R. Hovden, L. Brown, J. Park, D. A. Muller, P. L. McEuen, *Proc. Natl. Acad. Sci. U. S. A.* **2013**, 110, 11256.
- [16] S. K. Jain, V. Juričić, G. T. Barkema, *2D Mater.* **2017**, 4, 015018.
- [17] Y. Liu, J. N. B. Rodrigues, Y. Z. Luo, L. Li, A. Carvalho, M. Yang, E. Laksono, J. Lu, Y. Bao, H. Xu, S. J. R. Tan, Z. Qiu, C. H. Sow, Y. P. Feng, A. H. C. Neto, S. Adam, J. Lu, K. P. Loh, *Nat. Nanotechnol.* **2018**, 13, 828.
- [18] S. Y. Zhou, G. H. Gweon, J. Graf, A. V. Fedorov, C. D. Spataru, R. D. Diehl, Y. Kopelevich, D. H. Lee, S. G. Louie, A. Lanzara, *Nat. Phys.* **2006**, 2, 595.
- [19] S. Lisi, X. Lu, T. Benschop, T. A. De Jong, P. Stepanov, J. R. Duran, F. Margot, I. Cucchi, E. Cappelli, A. Hunter, A. Tamai, V. Kandyba, A. Giampietri, A. Barinov, J. Jobst, V. Stalman, M. Leeuwenhoek, K. Watanabe, T. Taniguchi, L. Rademaker, S. J. Van Der Molen, M. P. Allan, D. K. Efetov, F. Baumberger, *Nat. Phys.* **2021**, 17, 189.
- [20] A. Bostwick, F. Speck, T. Seyller, K. Horn, M. Polini, R. Asgari, A. H. MacDonald, E. Rotenberg, *Science* (80-.). **2010**, 328, 999.
- [21] D. Hsieh, Y. Xia, D. Qian, L. Wray, J. H. Dil, F. Meier, J. Osterwalder, L. Patthey, J. G. Checkelsky, N. P. Ong, A. V. Fedorov, H. Lin, A. Bansil, D. Grauer, Y. S. Hor, R. J. Cava, M. Z. Hasan, *Nature* **2009**, 460, 1101.
- [22] Y. L. Chen, J. G. Analytis, J. Chu, Z. K. Liu, S. Mo, X. L. Qi, H. J. Zhang, D. H. Lu, X. Dai, Z. Fang, S. C. Zhang, I. R. Fisher, Z. Hussain, Z. Shen, **2009**, 178, 1.
- [23] Z. K. Liu, B. Zhou, Y. Zhang, Z. J. Wang, H. M. Weng, D. Prabhakaran, S. Mo, Z. X. Shen, Z. Fang, X. Dai, Z. Hussain, Y. L. Chen, *Science* (80-.). **2014**, 343, 864.
- [24] P. Chen, W. W. Pai, Y. H. Chan, W. L. Sun, C. Z. Xu, D. S. Lin, M. Y. Chou, A. V. Fedorov, T. C. Chiang, *Nat. Commun.* **2018**, 9, 1.
- [25] Q. Peng, J. Zhou, C. Si, Z. Sun, *J. Alloys Compd.* **2019**, 788, 1113.
- [26] D. Hsieh, D. Qian, L. Wray, Y. Xia, Y. S. Hor, R. J. Cava, M. Z. Hasan, *Nature* **2008**, 452, 970.
- [27] C. X. Trang, Q. Li, Y. Yin, J. Hwang, G. Akhgar, I. Di Bernardo, A. Grubišić-Čabo, A. Tadich, M. S. Fuhrer, S. K. Mo, N. V. Medhekar, M. T. Edmonds, *ACS Nano* **2021**, 15, 13444.
- [28] J. L. Collins, A. Tadich, W. Wu, L. C. Gomes, J. N. B. Rodrigues, C. Liu, J. Hellerstedt, H. Ryu, S. Tang, S. K. Mo, S. Adam, S. A. Yang, M. S. Fuhrer, M. T. Edmonds, *Nature* **2018**, 564, 390.
- [29] Q. Li, C. X. Trang, W. Wu, J. Hwang, D. Cortie, N. Medhekar, S. K. Mo, S. A. Yang, M. T. Edmonds, *Adv. Mater.* **2022**, 34, DOI 10.1002/adma.202107520.
- [30] P. Nigge, A. C. Qu, Lantagne-Hurtubise, E. Mårzell, S. Link, G. Tom, M. Zonno, M. Michiardi, M. Schneider, S. Zhdanovich, G. Levy, U. Starke, C. Gutiérrez, D. Bonn, S. A. Burke, M. Franz, A. Damascelli, *Sci. Adv.* **2019**, 5, 1.
- [31] M. T. Edmonds, A. Tadich, A. Carvalho, A. Ziletti, K. M. O'Donnell, S. P. Koenig, D. F. Coker, B. Özyilmaz, A. H. C. Neto, M. S. Fuhrer, *ACS Appl. Mater. Interfaces* **2015**, 7, 14557.
- [32] Y. Liu, B. N. Shivananju, Y. Wang, Y. Zhang, W. Yu, S. Xiao, T. Sun, W. Ma, H. Mu, S. Lin, H. Zhang, Y. Lu, C. W. Qiu, S. Li, Q. Bao, *ACS Appl. Mater. Interfaces* **2017**, 9, 36137.
- [33] G. V. Bianco, M. Losurdo, M. M. Giangregorio, P. Capezzuto, G. Bruno, *Phys. Chem. Chem.*

- Phys.* **2014**, *16*, 3632.
- [34] M. Z. Iqbal, M. W. Iqbal, M. F. Khan, J. Eom, *Phys. Chem. Chem. Phys.* **2015**, *17*, 20551.
- [35] S. Hussain, M. W. Iqbal, J. Park, M. Ahmad, J. Singh, J. Eom, J. Jung, *Nanoscale Res. Lett.* **2014**, *9*, 1.
- [36] J. C. Yoon, P. Thiyagarajan, H. J. Ahn, J. H. Jang, *RSC Adv.* **2015**, *5*, 62772.
- [37] I. Gierz, J. Henk, H. Höchst, C. R. Ast, K. Kern, *Phys. Rev. B - Condens. Matter Mater. Phys.* **2011**, *83*, 1.
- [38] C. Q. Han, M. Y. Yao, X. X. Bai, L. Miao, F. Zhu, D. D. Guan, S. Wang, C. L. Gao, C. Liu, D. Qian, Y. Liu, J. Jia, **2014**, *085101*, 2.
- [39] J. Qiao, X. Kong, Z. X. Hu, F. Yang, W. Ji, *Nat. Commun.* **2014**, *5*, 1.
- [40] Y. Zheng, T. Ando, *Phys. Rev. B* **2002**, *65*, 1.
- [41] P. Huang, P. Zhang, S. Xu, H. Wang, X. Zhang, H. Zhang, *Nanoscale* **2020**, *12*, 2309.

FIGURES

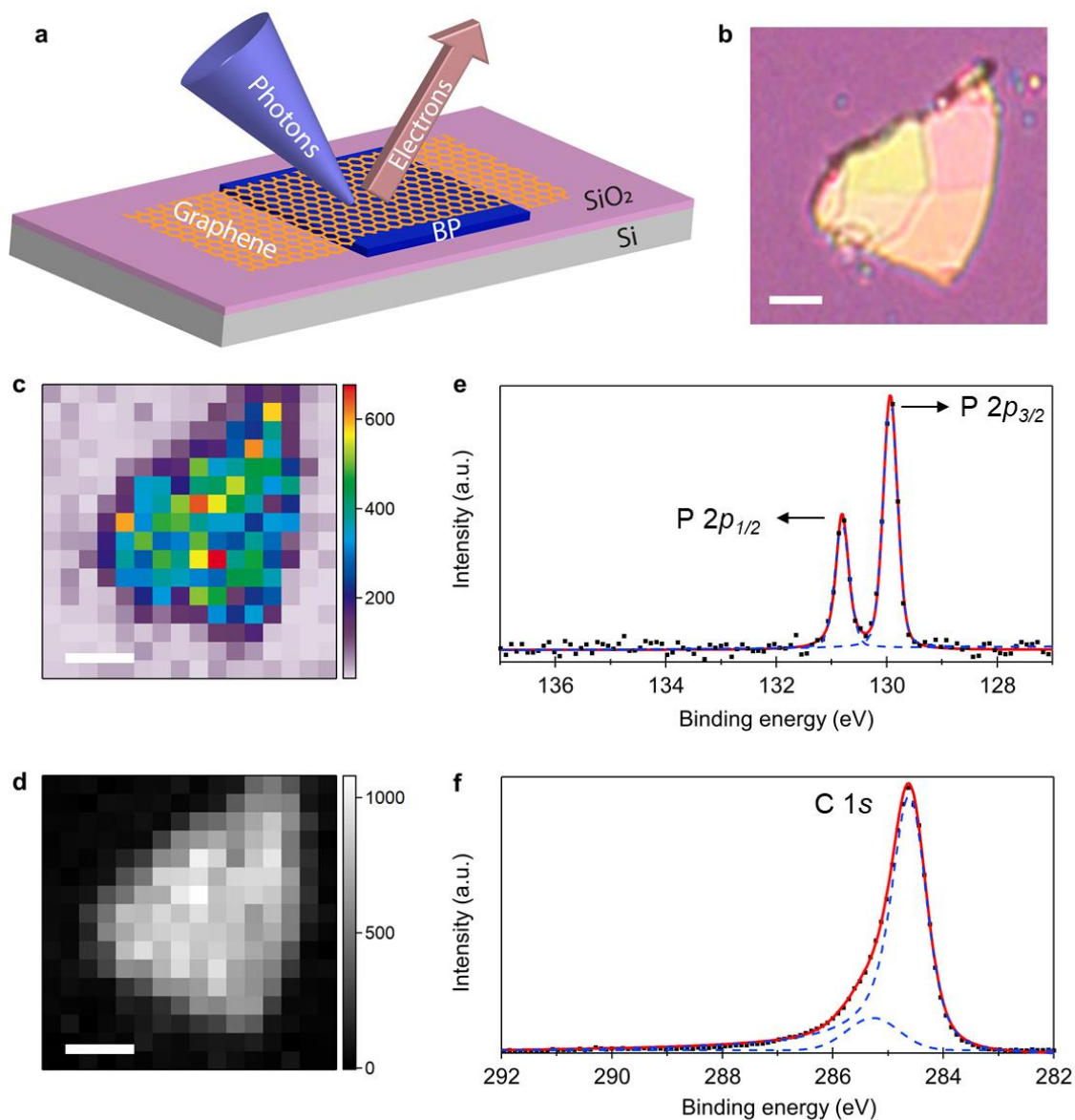


Figure 1. Basic characterisation of the G/BP heterostructure. **a**, Schematic of the heterostructure devices. **b**, Optical microscope image of the exfoliated Black phosphorus flake with CVD graphene on top. **c**, Spatial valence band mapping taken with photon energy of 150 eV. **d**, Spatial X-ray photoelectron spectroscopy mapping of P 2*p* peaks taken with photon energy of 200 eV. The scale bar in **b-d** is 50 μm . **e-f**, Core-level X-ray photoelectron spectroscopy of P 2*p* and C 1*s* core levels, respectively. The photon energies used in **e-f** are 200 eV and 350 eV, respectively.

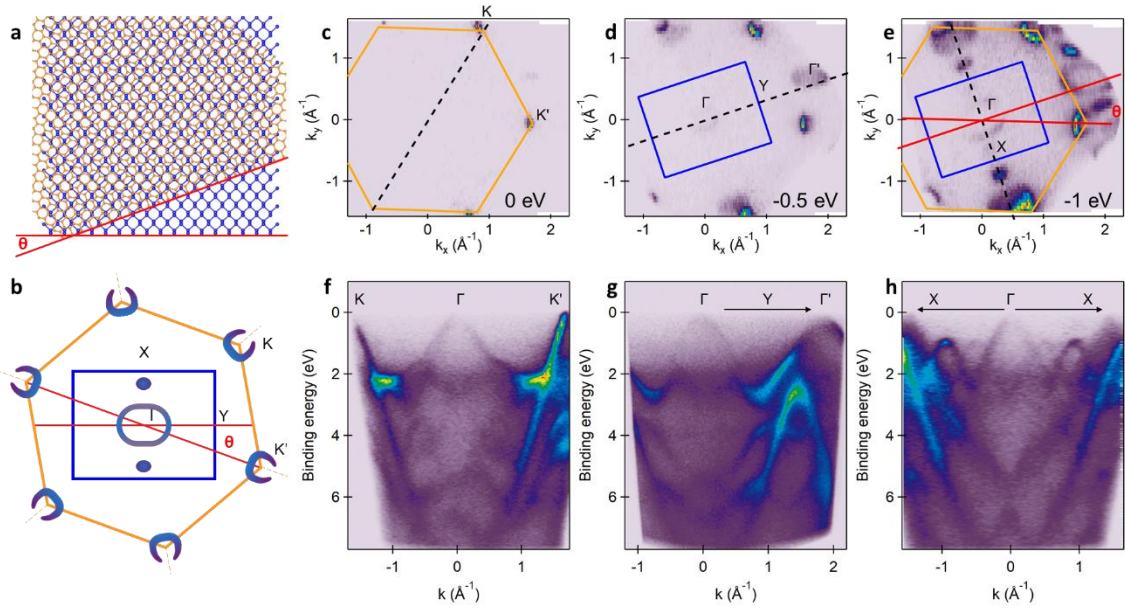


Figure 2. Overall electronic structure and iso-energy maps from nano-ARPES to determine the twist angle. **a**, Schematic of graphene (orange) on black phosphorus (blue) heterostructure highlighting the induced Moiré pattern. The rotation angle θ represents the angle between the nearest graphene zigzag direction and the black phosphorus zigzag direction. **b**, Schematic of graphene (orange) on black phosphorus (blue) first Brillouin zone and expected iso-energy contours. **c-e**, Iso-energy cuts taken at Fermi level, 0.5 eV and 1 eV below Fermi level, the surface Brillouin zones of graphene and black phosphorus are illustrated by the orange hexagon and blue rectangle, respectively. The K- Γ -K' direction of graphene and Γ -Y direction of black phosphorus in **e** are highlighted by red lines. **f-h**, Band dispersion along high symmetry directions marked by black dashed line in **c-e**, respectively. **f**, K- Γ -K' direction of graphene. **g**, Γ -Y direction of black phosphorus. **h**, Γ -X direction of black phosphorus.

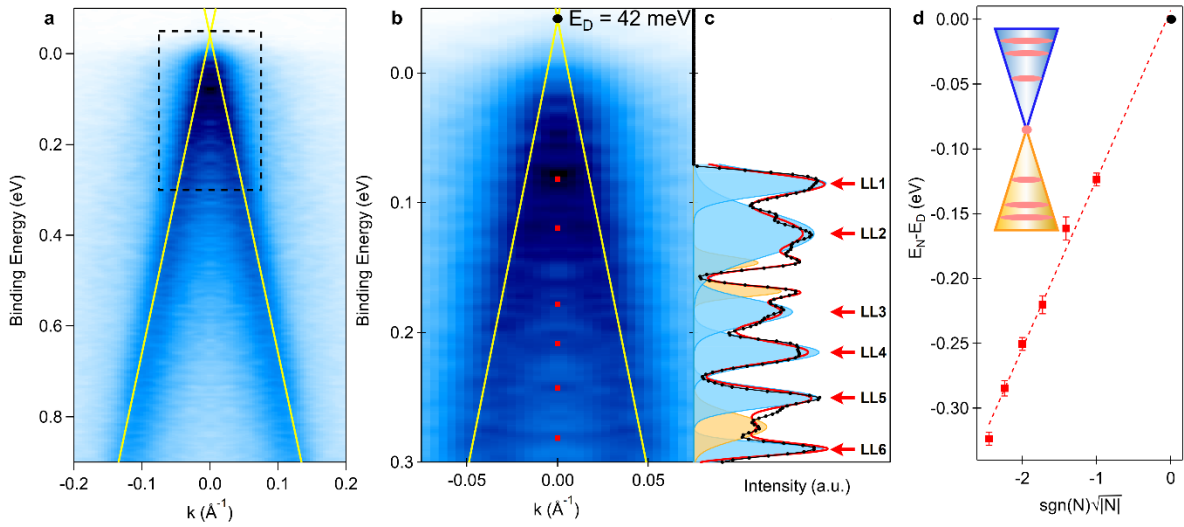


Figure 3. Visualisation of LLs in momentum space. **a**, High-resolution ARPES spectra at the K point to map the graphene Dirac cone. The linear dispersion of the Dirac cone is overlaid in yellow. The data has been reflected to compensate for matrix elements effects. **b**, High-resolution ARPES spectra at low energy as denoted by the black dashed box in **a**. The Landau level positions are marked as red squares. **c**, Energy distribution curve (black dots) extracted at the K point after subtracting the Fermi background, the red curve is from fitting to a series of Gaussian peaks. Blue peaks are peaks resulting from the dominant PMF and the orange peaks are from the non-uniform PMF in the heterostructure. The LLs in **c** are indicated by red arrows. **d**, Energy levels as a function of LLs index (red squares), the red line is a model fit of the data according to equation (3). The black circle represents the Dirac point, where an energy gap should be opened. The linear behaviour is consistent with LLs in a Dirac material.